

Negative Sample Matters: A Renaissance of Metric Learning for Temporal Grounding

Zhenzhi Wang, Limin Wang*, Tao Wu, Tianhao Li, Gangshan Wu
 State Key Laboratory for Novel Software Technology, Nanjing University, China

{zhenzhiwang, tianhaolee}@outlook.com, {lmwang, gswu}@nju.edu.cn, wt@smail.nju.edu.cn

Abstract

Temporal grounding aims to temporally localize a video moment in the video whose semantics are related to a given natural language query. Existing methods typically apply a detection or regression pipeline on the fused representation with a focus on designing complicated heads and fusion strategies. Instead, from a perspective on temporal grounding as a metric-learning problem, we present a Dual Matching Network (DMN), to directly model the relations between language queries and video moments in a joint embedding space. This new metric-learning framework enables fully exploiting negative samples from two new aspects: constructing negative cross-modal pairs from a dual matching scheme and mining negative pairs across different videos. These new negative samples could enhance the joint representation learning of two modalities via cross-modal pair discrimination to maximize their mutual information. Experiments show that DMN achieves highly competitive performance compared with state-of-the-art methods on four video grounding benchmarks. Based on DMN, we present a winner solution for STVG challenge of the 3rd PIC workshop. This suggests that metric-learning is still a promising method for temporal grounding via capturing the essential cross-modal correlation in a joint embedding space.

1. Introduction

Video analysis is a fundamental problem in computer vision and has drawn increasing attentions in recent years because of the potential applications in surveillance, robotics and Internet videos. While considerable progress has been made in video classification [66, 65, 11] and action localization [34, 36, 73, 83, 32], such tasks are still limited to recognize a pre-defined list of activities, such as playing baseball or peeling potatoes. As videos often contain complex activities that may cause combinatorial explosion if described by a list of actions and objects, the task of grounding language queries in videos [23, 12, 59],

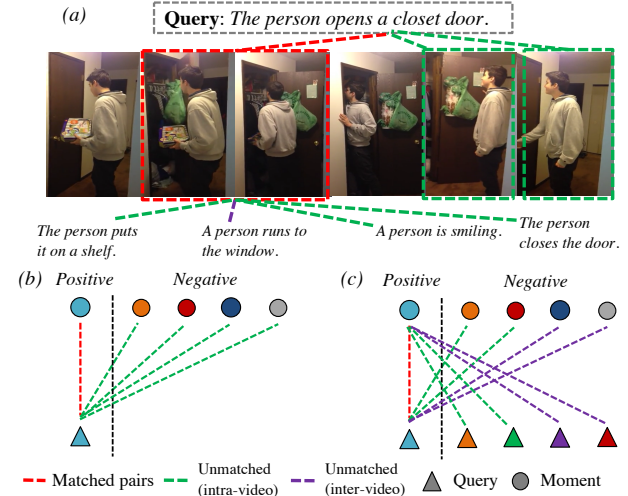


Figure 1. (a) In addition to matching moments by a given query, we propose a new auxiliary task named *dual matching* to differentiate the matched query (red dash line) among unmatched queries intra-video (green) or inter-video (purple) for the GT moment (red box). (b) Most previous methods only consider intra-video negative moments (green dash line). (c) Our *dual matching* uses negative pairs from both modalities intra-video (green dash line) or inter-video (purple dash line). **Best view with colors.**

as a generalization of the action localization task to overcome the constraints, has recently gained plenty of interest [23, 19, 12, 16, 79, 77, 75, 40, 82, 59] in both computer vision and language community. Formally, given a verbal description, the goal of temporal grounding is to determine the a temporal moment (i.e., the start and end time) that semantically corresponds to the query best in a given video.

Although temporal grounding opens up great opportunities for detailed video perception by using the new language modality to capture the complex relations between sentences and videos, most of previous approaches [79, 75, 82, 77, 59] still tackle this problem in a *detection/regression* way with *early-fusion* designs, e.g., using the fused multi-modal features to predict the offset of action moments from anchors; or directly regressing the desired region on a globally aggregated multi-modal feature. These indirect ground-

*Limin Wang is the corresponding author.

ing methods typically ignore the essential relation between all cross-modal pairs (i.e., pairs of moment and language queries), and they only simply utilize the IoU-based score between the given sentence and moments from the *same video* as supervision (Fig. 1(b)). However, we argue that the negative relations between the given moment and other *unmatched descriptions* are also important for learning a joint cross-modal embedding. Intuitively, the auxiliary task that given a video moment with visually informative actions, training the model to contrast the matched query and unmatched descriptions (Fig. 1(a)) is beneficial for temporal grounding task. We propose to use this auxiliary task for the first time in temporal grounding, which shows advantages in less extra computational cost compared with previous auxiliary tasks. In order to model such relations from dual directions (Fig. 1(c)), we revisit temporal grounding task from a *metric learning perspective*, which allows us to directly model the essential similarity measurement in a joint cross-modal embedding space, rather than designing sophisticated detection/regression strategies based on the fused representation as in many previous methods.

In our metric-learning view, sentences and video moments play an equally important role in temporal grounding and both matching directions are adopted, i.e., select the right instance in a modality given the other modality. The supervision signals are in a symmetric form for two modalities (Fig. 1(c)), so more supervision signals than previous methods are constructed by our approach. Our framework shows several advantages: Firstly, our metric-learning perspective enables us to mining negative samples from a *dual matching scheme*. In this sense, an *unmatched relations* is also informative by implying that these moments and sentences should be pushed away in the joint embedding space. To achieve this, we adopt a cross-modal pair discrimination objective to contrast pos/neg moment-sentence pairs inspired by a cross-modal pretraining method [31]. Secondly, we exploit more negative samples to improve our representation learning from *inter-video* negative samples by adopting our dual matching scheme. In contrast to most of previous methods which only utilize *intra-video* moment-sentence pairs as supervision due to the fused multi-modal feature, our architecture can also take advantage of the *inter-video* pairs. Finally, we model the visual and language feature in a Siamese-alike network architecture with different encoders for each modality and a simple dot-product is utilized for similarity computation. In this way, our framework has less training cost by sharing moment features among sentences inside each video.

While using the negative pairs can lead to a better feature, the binary supervision signal itself (i.e., matched or unmatched) is still too weak to rank the moments inside a video. In addition, although the negative pairs used in our dual matching scheme provide much more supervision

signals, most of them are easy negatives (especially the inter-video ones). So we adopt another embedding space for learning the cross-modal similarity for precisely ranking moments based on the IoU supervision, which enables us to estimate finer relations (i.e., a scalar instead of a binary signal) and accurately differentiate the correct pair among hard negatives (e.g., negative moments with high IoU). These two complementary objectives share the same feature encoders as backbone and have their own customized heads.

Our main contributions are three-fold: (1) We revisit the metric learning perspective on the temporal grounding task in a *late-fusion* fashion¹ and leverage **inter-video** negative visual-language pairs. Our framework shows advantages on both performance and training cost. (2) Our metric learning view enables a new auxiliary task for temporal grounding, named **cross-modal dual matching**. Instead of heavy additional networks for previous auxiliary tasks, ours has a more direct idea and is also more effective. (3) We conduct comprehensive quantitative and qualitative analyses on four benchmarks and reveal some interesting findings.

2. Related Works

2.1. Temporal Grounding

Temporal grounding task aims to retrieve the video moment by a given language query. Previous methods can be mainly categorized as four groups: (1) **Regression methods** directly predict the boundaries (i.e., start and end) of the target moment from the fused multi-modal features relying on either a clip-wise boundary classification in local regions [16, 43, 80, 4], or a direct boundary regression on the aggregated global feature [76, 64, 42]. Some methods also introduce some heuristics, e.g., aggregating clip-wise actionness scores modeled by compositional reasoning [38] or taking the expectation of probability for start/end [16]. (2) **Detection methods** often first generate candidate moments and then evaluate them on the fused multi-modal features [12, 14]. Their evaluation on moments utilize various designs, e.g., LSTM [3, 72], dynamic filtering [79, 43] or modulation [75], graph convolution [79], anchor-free detectors [40, 77], and 2D moment map [82]. (3) **Reinforcement Learning methods** [19, 67, 69] localize the target moment iteratively by defining the *state* and *action* on the video and treating this task as a sequential decision making process. (4) The only previous **metric learning method** [23] use a triplet loss with ℓ_2 distance as the similarity measurement to match the given sentence to the correct video moment. However, it lacks both the important supervision of negative sentence samples, i.e., our novel *dual matching scheme* and the effective relation modeling of moments. Therefore its performance is much worse than ours.

Multi-modal fusion. Many methods from the group 1) to 3)

¹Please refer to Appendix A.3. for analysis of early/late-fusion.

mainly adopt a *early-fusion* pipeline for cross-modal modeling, e.g., by concatenation [3, 37, 64], dynamic convolution [43, 79] or modulation [75], cross-attention [40, 78], and hadamard product [77, 42, 82]. On the contrary, we use a simple inner-product in the joint visual-language space to measure the cross-modal similarity in a *late-fusion* manner. Our late-fusion strategy not only enables our dual matching scheme, but also shows advantages in computational cost during training by sharing the video feature among sentences in the same video.

Auxiliary tasks in temporal grounding. Previous methods [37, 72] has explored the usage of query reconstruction as an auxiliary task for temporal grounding by adding a video caption loss following image-based grounding methods [49, 46]. Yet it introduces extra overhead of network parameters and computational cost, e.g., LSTM [72] or Transformer [37]. Our proposed auxiliary task of dual matching avoid the usage of the heavy additional network and is also more direct.

2.2. Spatio-temporal temporal grounding

As the recent progress achieved in spatio-temporal action detection [32], spatio-temporal temporal grounding task [59] is also proposed to be an extended spatio-temporal version of temporal grounding. By adopting our proposed DMN on the linked human bounding boxes [27] for temporal trimming, we show significant performance gains over the previous transformer-based method [59].

2.3. Metric Learning

The family of metric learning loss has been explored to learn powerful representations with the classification setting [18, 54, 55, 29], where the positive sample is chosen from the same class and the negative one from other classes; or self-supervised setting [62, 7, 20, 70, 24], which select positive samples using data augmentation or co-occurrence. Different from both setting, we choose pos/neg cross-modal pairs according to the groundtruth in a *supervised* way. Yet, our dual matching scheme has *no pre-defined categories*, but binary classes for cross-modal pairs, i.e., matched or unmatched. Therefore we adopt cross-modal pair discrimination [31] similar to instance discrimination [70], where each instance defines an unique class. In addition, most aforementioned methods use single-modal samples, e.g., images, while we utilize cross-modal moment-sentence pairs. There are some video-language pre-training methods [31, 41] similar to our setting, yet they aim to learn *video-level* representations in an *unsupervised* way while we want to enhance *proposal-level* features in a *supervised* way, where no pre-training dataset is used in our approach.

3. Model

As discussed in Sec. 1, our DMN proposes to use negative sentence samples to construct a dual matching scheme from the metric learning prospective. To enable this auxiliary task, we adopt a late modality fusion with advantages in less computational cost than baseline [82]. Sec. 3.1 introduces the formulation of temporal grounding. Sec. 3.2 illustrates how to construct our DMN from the baseline [82]. Then, we analyze the two complementary loss of IoU regression and cross-modal pair discrimination in Sec. 3.3.

3.1. Problem Formulation

Given an untrimmed video V and a natural language query S , the temporal grounding task aims to localize a temporal moment (x_s, x_e) that matches the query. We denote the video as a sequence of frames $V = \{x_i\}_{i=1}^{l_v}$, where x_i is a frame and l_v is the total number of frames; the query sentence as a sequence of words $S = \{s_i\}_{i=1}^{l_s}$, where s_i is a word and l_s is the total number of words. Ideally, the retrieved moment (x_s^*, x_e^*) should deliver the same semantic as the sentence S . We adopt the feature vectors in the joint space to represent sentence S and moments (x_i, x_j) , therefore the inner product of visual and text features after ℓ_2 -norm should be maximized.

3.2. Architecture

Our DMN adopts a Siamese-alike network architecture with a late modality fusion by a simple inner product in the joint visual-language space, as illustrated in Fig. 2.

Language Encoder. Previous works commonly utilize a LSTM [25] upon a sequence of word vectors embedded by GloVe [45]. Yet, some concerns about unfair comparisons in previous methods² motivate us to adopt a standard language encoder. We choose DistilBERT [51] for its light-weight model capacity. For each input sentence S , we first generate the tokens of words by the tokenizer and add a class embedding token ‘[CLS]’ in the beginning. Then we feed the tokens into DistilBERT to get a feature sequence $\{\mathbf{f}_i^S\}_{i=1}^{l_s+1}$, where $\mathbf{f}_i^S \in \mathbb{R}^{d^S}$ and $d^S=768$ is the feature dimension. There are two commonly used aggregation approaches to get the whole sentence’s embedding: 1) global average pooling over all tokens; 2) the class embedding ‘[CLS]’. Our experiment shows that global average pooling has faster convergence and better performance in this task, so we take average pooling as default.

Video Encoder. We extract features of the input video and encodes them as a 2D temporal moment feature map following the baseline 2D-TAN [82]. We segment the input video stream into small video clips $\{v_i\}_{i=1}^{l_v/t}$ with each clip v_i containing t frames, then extract clip-level features

²For example, GloVe models pre-trained on different corpuses, and bi-directional or not. Please see appendix B.2.1 for details.

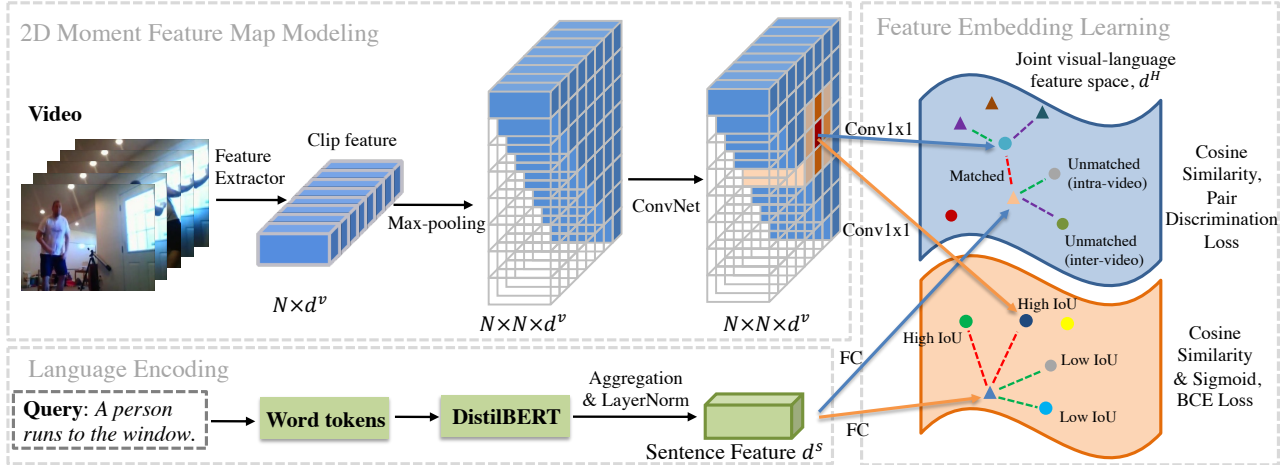


Figure 2. Overview of our framework. Different from the baseline, we adopts a late modality fusion strategy and learning the feature embedding for moments and sentences on two independent spaces with pair discrimination and BCE losses, respectively. The dots and triangles are the feature of moments and sentences. The red dash lines are matched moment-sentence pairs to be pulled in, while green/purple dash lines are negative samples intra/inter-video to be pushed away. **Best view with colors.**

with an off-the-shelf pre-trained CNN model (e.g., C3D). We perform a fixed-length sampling to obtain N clip-level features for each video by a even stride $\frac{l_v}{t \cdot N}$ and pass the fixed-length features through a FC layer to reduce their dimension, denoted as $\{\mathbf{f}_i^V\}_{i=1}^N$, where $\mathbf{f}_i^V \in \mathbb{R}^{d^V}$. Then we build up the 2D feature map for candidate moments following the baseline [82] as $\mathbf{F}^M \in \mathbb{R}^{N \times N \times d^V}$, where we adopt the max-pooling as the moment-level feature aggregation strategy following. We also utilize the sparse sampling strategy which removes highly overlapped moments to reduce the number of candidate moments as well as computation cost³. Different from 2D-TAN [82], we directly model the relations of moments $\mathbf{F} \in \mathbb{R}^{N \times N \times d^V}$ by L layers of 2D convolution with kernel size K only based on visual features. As discussed in [44], the performance of 2D-TAN has no significant drop when the order of input video clips is randomly permuted (i.e., the ‘sanity check’), which is counter-intuitive. It indicates that to some extent 2D-TAN ignores the visual features and overfits the bias in the dataset, such as temporal distributions of actions conditioned on sentences. The design of our DMN forces the convolution filters to actually utilize the visual features.

Joint Visual-Language Embedding. Finally, we estimate the matching quality of each moment based on the similarity of two modalities for both supervision signals (i.e., IoU regression and cross-modal pair discrimination). We adopt a LayerNorm [1] for more stable convergence in language feature aggregation. We use a linear projection layer or a 1x1 convolution to project the language and visual features into the same dimension d^H respectively. The final representations of sentence feature are $\mathbf{f}_{pd}^S, \mathbf{f}_{iou}^S \in \mathbb{R}^{d^H}$ for

³Please see appendix A.1. for the details of sparse sampling.

cross-modal pair discrimination (subscript pd) and IoU regression (subscript iou). Moment features are $\mathbf{F}_{pd}^V, \mathbf{F}_{iou}^V \in \mathbb{R}^{N \times N \times d^H}$.

$$\mathbf{f}^S = \text{LayerNorm}(\mathbf{f}_0^S) \text{ or } \text{LayerNorm}\left(\frac{1}{N} \sum_{i=1}^{l_s+1} \mathbf{f}_i^S\right) \quad (1)$$

$$\mathbf{f}_{pd}^S = \mathbf{W}_{pd} \mathbf{f}^S + \mathbf{b}_{pd}, \quad \mathbf{f}_{iou}^S = \mathbf{W}_{iou} \mathbf{f}^S + \mathbf{b}_{iou} \quad (2)$$

$$\mathbf{F}_{pd}^V = \text{conv}_{pd}(\mathbf{F}, 1, 1), \quad \mathbf{F}_{iou}^V = \text{conv}_{iou}(\mathbf{F}, 1, 1) \quad (3)$$

where \mathbf{W} . and \mathbf{b} . are learnable parameters, $\text{conv.}(\mathbf{x}, k, s)$ is 2D convolution with kernel size k and stride s for 2D feature map \mathbf{x} . The subscripts id or iou means the weights of two branches are independent. Then we regard the cosine similarity as moments’ estimation scores for both losses.

$$\begin{aligned} \forall \mathbf{f}_{pd}^V \in \mathbf{F}_{pd}^V, s^{pd} &= \mathbf{f}_{pd}^{V\text{T}} \mathbf{f}_{pd}^S \\ \forall \mathbf{f}_{iou}^V \in \mathbf{F}_{iou}^V, s^{iou} &= \mathbf{f}_{iou}^{V\text{T}} \mathbf{f}_{iou}^S \end{aligned} \quad (4)$$

where we enforce the embedding $\|\mathbf{f}^V\|_2 = \|\mathbf{f}^S\|_2 = 1$ via a ℓ_2 -normalization layer.

3.3. Loss Functions

Our DMN integrates two complementary losses: a binary cross entropy loss for regressing the IoU and a pair discrimination loss for learning discriminative features.

Binary Cross Entropy (BCE) Loss. We follow 2D-TAN [82] to adopt the scaled IoU values y_i for each candidate moments as the supervision signal, as shown in Tab. 1 (IoU regression). The IoU values are linearly scaled from (t_{min}, t_{max}) to $(0, 1)$ and truncate the values beyond $(0, 1)$. We directly use the value of t_{min} and t_{max} reported in 2D-TAN, which is . We notice that the range of cosine similarity is $s^{iou} \in (-1, 1)$, yet the IoU signal is $y_i \in (0, 1)$. So

we adopt a commonly-used sigmoid function σ to highlight the value change near the neutral region (e.g., $y_i=0.5$). We heuristically amplify the s^{iou} by a factor of 10 to make the range of final prediction of our model $p_i^{iou} = \sigma(10 \cdot s_i^{iou})$ cover most of the regions in $(0, 1)$. The regression branch of our DMN is trained by a BCE loss:

$$L_{bce} = -\frac{1}{C} \sum_{i=1}^C \left(y_i \log p_i^{iou} + (1 - y_i) \log(1 - p_i^{iou}) \right) \quad (5)$$

where p_i^{iou} is the final score of a moment and C is the total number of valid candidates.

Cross-modal Pair Discrimination. As discussed in Sec. 1, our dual matching scheme creates more supervision signals for temporal grounding by cross-modal pair discrimination. By contrasting the positive moment-sentence pairs with the negative ones sampled from *both intra and inter videos*, encoders will learn a more discriminative features for both modalities *without any extra pre-training dataset*. As shown in Tab. 1, our pair discrimination objective introduces two novel aspects for supervision signals: 1) pair of ground-truth moment with pos/neg sentences (row 2); and 2) inter-video pairs (column 7). In contrast, previous detection/regression methods only sample pos/neg samples based on IoU signals (row 3), and the previous metric learning method [23] only has single direction of matching (row 1) yet lacks the important dual matching scheme (row 1 and row 2). Specifically, our pair discrimination aims to learn features for moments \mathbf{f}_{pd}^V and sentences \mathbf{f}_{pd}^S , where these features should be similar if the moment-sentence pair is semantically matched and dissimilar if it is semantically unrelated. We adopts the following conditional distribution in a non-parametric softmax form:

$$p(i_s|v) = \frac{\exp((\mathbf{f}_i^{ST}\mathbf{f}^V - m)/\tau_v)}{\exp((\mathbf{f}_i^{ST}\mathbf{f}^V - m)/\tau_v) + \sum_{j \neq i}^{N_s} \exp(\mathbf{f}_j^{ST}\mathbf{f}^V/\tau_v)} \\ p(i_v|s) = \frac{\exp((\mathbf{f}_i^{VT}\mathbf{f}^S - m)/\tau_s)}{\exp((\mathbf{f}_i^{VT}\mathbf{f}^S - m)/\tau_s) + \sum_{j \neq i}^{N_v} \exp(\mathbf{f}_j^{VT}\mathbf{f}^S/\tau_s)} \quad (6)$$

where the i^{th} sentence or moment define a instance-level class i_s or i_v , the feature embedding \mathbf{f}^S and \mathbf{f}^V are ℓ_2 normalized, τ_s and τ_v are temperatures and N_s and N_v are total numbers of sampled instances in the batch. Although the conditional distribution of video moments and sentences are similar, their differences are non-trivial due to the selection of negative samples, i.e., $N_v - 1$ negative video moments are sampled from low IoU moments inside videos or moments from other videos; and $N_s - 1$ negative sentences are sampled from other sentences in the video or from other videos. To enable a steady training process, we only adopt the moments whose IoU with ground-truth moment lower than a threshold as negative samples (e.g., ≤ 0.5). To further reduce the potential false negative signals, the sentences similar to the ground-truth sentence is automatically removed from the negative sample set, i.e., by computing their matched moments' IoU with ground-truth moment and removing them if their IoU ≥ 0.5 . When

Loss	Modality	IoU with GT (moment or its corrs. sentence)				
		1	(0.5, 1)	(0, 0.5)	0	other video
Pair discrimination	vid.	pos.	-	neg.	neg.	neg.
	sent.	pos.	-	neg.	neg.	neg.
IoU regression	vid.	max	high	low	min	-

Table 1. Supervision signals of our DMN. We categorize moments/sentences as pos./neg. samples according to IoU of this moment (or this sentence’s corresponding moment) with the GT moment. We introduce two novel types of supervisions: 1) negative sentence samples in pair discrimination (row 2), and 2) inter-video negatives (column 7).

we construct the negative sample set, we hold an assumption that only a small portion of inter-video negative samples (both sentences and moments) will semantically close to the positive sample. It is reasonable if the size of training video corpus is large enough.

The objective of our pair discrimination is to maximize the likelihood $\prod_{i=1}^N p(i_s|v_i) \prod_{i=1}^N p(i_v|s_i)$ where N is the total number of moment-sentence pairs for training. The cross-correlation enables the network to effectively capture the mutual information between modalities by guiding the learning process of feature representation learning with the binary pair supervision. The loss function is as follows

$$L_{pd} = - \left(\sum_{i=1}^N \log p(i_v|s_i) + \sum_{i=1}^N \log p(i_s|v_i) \right) \quad (7)$$

Our final loss function L is a linear combination of binary cross entropy loss and pair discrimination loss, and the final prediction score s for candidate moments given the query sentence are these two scores’ product.

$$L = L_{bce} + \lambda L_{pd}, \quad s = s^{iou} \cdot s^{pd}. \quad (8)$$

4. Experiments

4.1. Datasets

ActivityNet-Captions [30] is built on ActivityNet v1.3 dataset [22], which covers a wide range of complex human actions. It is originally designed for video captioning and recently introduced into temporal grounding. There are 37,417, 17,505, and 17,031 moment-sentence pairs for training, validation and testing. Following the setting of 2D-TAN [82], we report the evaluation result on val_2 set.

TACoS consists of 127 videos selected from the MPII-Cooking dataset [50]. It is comprised of 18,818 video-language pairs of different cooking activities in the kitchen annotated by Regneri *et al.* [47]. A standard split [12] consists of 10,146, 4,589, and 4,083 moment-sentence pairs for training, validation and testing, respectively. We report evaluation results on test set in our experiments.

Charades-STA [12] is an extended version of action recognition and localization dataset Charades [52] by Gao *et al.* [12] for temporal grounding. It contains 5,338 videos and

12,408 query-moment pairs in the training set, and 1,334 videos and 3,720 query-moment pairs in the test set.

HC-STVG [59] dataset is introduced to localize an action tubelet of the target person spatio-temporally from an untrimmed video based on a given textual description. It contains 5,660 videos selected from AVA [17] where each video has one video-sentence pair. A standard split consists of 4,500 pairs for training and 1,160 pairs for testing.

We also observe some inconsistent settings or unfair comparisons among previous works, so we call for standardization in experiments, e.g., reduce the usage of I3D feature. Please refer to appendix B.3. for details.

4.2. Experimental Settings

Evaluation Metrics. Following previous setting [12] of *temporal grounding*, we evaluate our model by computing *Rank n@m*. It is defined as the percentage of sentence queries having at least one correctly localized moment, i.e. $\text{IoU} \geq m$, in the top- n retrieved moments. There are specific settings of n and m for different datasets. Specifically, we report the results as $m \in \{0.5, 0.7\}$ for Charades-STA, $m \in \{0.1, 0.3, 0.5\}$ for TACoS and $m \in \{0.3, 0.5, 0.7\}$ for ActivityNet Captions dataset with $n \in \{1, 5\}$. For *spatio-temporal video grounding*, we report mean of vIoU and vIoU@{0.3, 0.5} following HC-STVG benchmark [59], where vIoU is computed by the top-1 predicted tube with the GT tube (see Appendix A.5.1 for the details of metrics.).

Implementation Details. We adopt standard off-the-shelf video feature extractors without fine-tuning in each dataset. Our convolution network for 2D proposal feature modeling uses the same settings with 2D-TAN [82] (max-pool version) for fair comparisons. Our language encoder is a light-weighted DistilBERT [51] for better standardization (see Appendix B.1.) and we also show the performance of our DMN with LSTM (Appendix B.2.2.). Each mini-batch has B videos instead of B moment-sentence pairs, where B is batch size. Please see Appendix A.2. for more details about hyper-parameters. For details of how we adapt our DMN to handle spatio-temporal video grounding task, please refer to Appendix A.5.2.

4.3. Ablation Study

In this section, we evaluate the effects of some key components in our proposed DMN, where the most important part is ablations of our proposed dual matching scheme. Due to the limit of pages, please refer to Appendix B for other ablations, e.g., impact of DistilBERT (B.1.) and comparisons between our DMN and 2D-TAN decomposed by moment length (B.4.).

Cross-modal Pair Discrimination. We investigate the most of important part in our method, i.e., ‘cross-modal pair discrimination’, by ablating different types of negative samples on both Charades-STA and ActivityNet Cap-

BCE	intra-video		inter-video		R@1		R@5	
	vid.	sent.	vid.	sent.	IoU0.5	IoU0.7	IoU0.5	IoU0.7
✓					40.12	23.89	79.57	53.26
✓	✓				40.65	24.49	77.98	55.89
✓	✓	✓			43.36	26.48	81.85	57.24
✓			✓	✓	46.32	26.59	83.41	56.77
✓	✓	✓	✓		45.13	26.24	83.69	58.13
✓	✓	✓		✓	46.91	27.46	83.09	58.36
✓	✓	✓	✓	✓	44.70	24.92	79.76	53.71
✓	✓	✓	✓	✓	47.31	27.28	83.74	58.41

BCE	intra-video		inter-video		R@1		R@5	
	vid.	sent.	vid.	sent.	IoU0.3	IoU0.5	IoU0.3	IoU0.5
✓					62.73	46.74	27.12	85.67
✓	✓				62.27	46.43	27.75	85.80
✓	✓	✓			63.41	47.52	29.69	86.37
✓			✓	✓	64.64	48.26	28.75	86.52
✓	✓	✓	✓		64.01	47.47	28.89	87.38
✓	✓	✓		✓	64.25	48.24	28.96	86.65
✓	✓	✓	✓	✓	63.47	45.28	26.29	85.55
✓	✓	✓	✓	✓	65.05	48.59	29.26	87.25
							79.50	64.76

Table 2. Ablation on negative samples in pair discrimination. (top) Charades-STA results; (bottom) ActivityNet Captions results. Intra/inter-video means we use video moments (vid.) or sentences (sent.) inside or cross videos as negatives.

Method	R@1			R@5		
	IoU0.3	IoU0.5	IoU0.7	IoU0.3	IoU0.5	IoU0.7
Only Intra	63.41	47.52	29.69	86.37	78.17	62.50
#neg. = Intra	64.18	47.55	28.48	86.74	79.01	64.15
Intra + Inter	65.05	48.59	29.26	87.25	79.50	64.76

Table 3. Ablation on number of negatives (ActivityNet-Captions).

tions datasets, as shown in Tab. 2. Row 1 is the baseline of our model for not using pair discrimination. Row 2 uses the same information with previous works (e.g., intra-video moment negatives), which shows similar performance with row 1. By introducing sentence negatives, notable performance gain is observed in row 3 to row 6 when comparing to row 1 and row 2. It proves the effectiveness of our dual matching scheme. Besides, we conclude some observations based on the differences inside row 3 to row 8: (1) Due to the larger number of negatives, only using inter-video negatives (row 4) tend to be more effective than only using intra-video negatives (row 3), especially in smaller datasets (e.g., Charades-STA); (2) Best results are often obtained by both intra and inter-video negatives (row 8), and sub-optimal results are often achieved in row 5 and 6 by discarding some specific type of inter-video negatives. It indicates hard negative mining of inter-video samples could be further investigated; (3) Only using our pair discrimination achieves similar or better performance than original BCE loss in two datasets (row 7 vs. row 1), demonstrating the powerful additional supervision signals introduced by our dual matching scheme.

Number vs. Type of Negative Samples. We have shown inter-video negatives are beneficial by introducing much more negatives than previous methods in Tab. 2. However, whether the number or the type of negatives is more important in our method? To ablate this, we construct a baseline that randomly picks the same numbers of negatives with

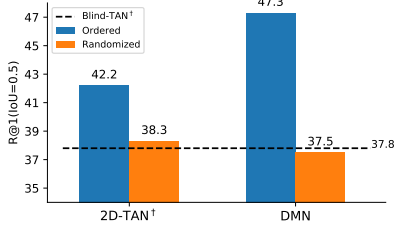


Figure 3. Sanity Check on the Charades-STA dataset. \dagger values are obtained from [44].

Charades-STA	R@1		R@5	
	IoU0.5	IoU0.7	IoU0.5	IoU0.7
Class Embedding ‘CLS’	45.11	27.25	82.37	58.09
Average Pooling	47.31	27.28	83.74	58.41

Table 4. Ablation on text feature aggregations.

Hyper-parameters	R@1		R@5	
	IoU0.5	IoU0.7	IoU0.5	IoU0.7
$m = 0.3$	45.30	27.13	83.33	59.02
$m = 0.4$	47.31	27.28	83.74	58.41
$m = 0.5$	46.32	26.82	83.09	58.10
$\lambda = 0.05$	47.31	27.28	83.74	58.41
$\lambda = 0.1$	45.63	27.13	83.34	57.33
$\lambda = 0.2$	44.91	26.95	82.97	57.69
$\tau_v = \tau_s = 0.1$	47.31	27.28	83.74	58.41
$\tau_v = \tau_s = 0.2$	43.88	25.81	82.23	57.55

Table 5. Ablation on Hyper-parameters (Charades-STA).

intra-video negatives among all intra and inter-video negatives (row 2). Therefore, it uses the **same** number with only intra-video negatives (row 1) *in each iteration* yet will eventually see more types of negatives in the entire training process. As shown in Tab. 3, the performance of this baseline (row 2) is similar to only using intra-video negatives (row 1) in R@1 metrics and is better in R@5 metrics, indicating the importance of more types of negatives introduced by our dual matching scheme.

Aggregation of Language Feature. In Tab. 4, we compare two aggregation strategies for the sentence feature. While many methods in NLP including BERT [10] directly adopt the class embedding as the representation of the whole sentence, we find the average pooling over all words is more robust in our task. It indicates that the scale of video grounding datasets is limited in vocabulary size or annotated sentences, e.g., TACoS dataset only has a vocabulary size of 2255 words and a training set of 10146 sentences, while NLP pre-training datasets commonly have millions of sentences. We empirically use average pooling as default.

Hyper-parameters. In Tab. 5, we ablate some important hyper-parameters, including margin m , temperature τ_s and τ_v and weight λ of pair discrimination loss. Due to the small size of Charades-STA, they do have a little influences but have no notable change of the gap between ours and baseline [82]. We set them by just a few tries on each dataset.

Sanity Check on Visual Input. In [44], the authors observe that the blind baselines which only uses training set priors or conditional distributions of moments given queries already outperform many previous state-of-the-art methods.

Method	R@1			R@5		
	IoU0.3	IoU0.5	IoU0.7	IoU0.3	IoU0.5	IoU0.7
MCN [23]	39.35	21.36	6.43	68.12	53.23	29.70
CTRL [12]	47.43	29.01	10.34	75.32	59.17	37.54
ACRN [38]	49.70	31.67	11.25	76.50	60.34	38.57
QSPN [72]	52.13	33.26	13.43	77.72	62.39	40.78
ABLR [76]	55.67	36.79	—	—	—	—
SCDM [75]	54.80	36.75	19.86	77.29	64.99	41.53
PMI [5]	59.69	38.28	17.83	—	—	—
LGI [42]	58.52	41.51	23.07	—	—	—
CMIN [37]	<u>63.61</u>	44.62	24.48	82.39	69.66	52.96
DRN [77]	—	<u>45.45</u>	24.39	—	<u>77.97</u>	50.30
2D-TAN [82] [†]	59.46	44.51	<u>26.54</u>	<u>85.53</u>	77.13	61.96
Our DMN	65.05	48.59	29.26	87.25	79.50	64.76

Table 6. Performance comparison on ActivityNet Captions (C3D feature). [†]we use max-pool version of 2D-TAN for comparison.

Method	R@1			R@5		
	IoU0.1	IoU0.3	IoU0.5	IoU0.1	IoU0.3	IoU0.5
MCN [23]	14.42	—	5.58	37.35	—	10.33
CTRL [13]	24.32	18.32	13.30	48.73	36.69	25.42
QSPN [72]	25.31	20.15	15.23	53.21	36.72	25.30
SM-RL [67]	26.51	20.25	15.95	50.01	38.47	27.84
SLTA [26]	23.13	17.07	11.92	46.52	32.90	20.86
ABLR [76]	34.70	19.50	9.40	—	—	—
SCDM [75]	—	26.11	21.17	—	43.35	28.53
CMIN [37]	36.68	27.33	19.57	64.93	40.16	32.18
DRN [77]	—	—	23.17	—	—	33.36
2D-TAN [82]	<u>47.59</u>	<u>37.29</u>	<u>25.32</u>	<u>70.31</u>	<u>57.81</u>	<u>45.04</u>
Our DMN	51.39	39.24	26.17	78.03	62.03	47.39

Table 7. Performance comparison on TACoS (C3D feature).

So they further examine the contribution of visual inputs by evaluating the performance gap between the ordered input clips and randomly shuffled input clips, named as ‘sanity check’. We follow this setting to check our method on Charades-STA in Fig. 3: Our model with randomized visual input predicts a even lower result (37.5 vs. 37.8) than Blind-TAN [44] which does not use any visual input. Our performance gap between ordered inputs and shuffled inputs is also larger than 2D-TAN’s, which means our DMN shows better result in this sanity check. It indicates our method better exploits visual information.

4.4. Comparison with State-of-the-Art

Temporal grounding. We achieve good results on three datasets: ActivityNet Captions, Charades-STA and TACoS as reported in Tab. 6, Tab. 8, and Tab. 7. The top-2 performance values in tables are highlighted by bold or underline. Due to the concerns about unfair comparisons analyzed in appendix B.3., we do not compare the results with I3D features on Charades-STA and only focus on the standard feature on the official website (i.e., VGG feature). Our proposed DMN outperforms the strong baseline [82] with a significant margin by leveraging our dual matching scheme (i.e., using both video and sentence negative samples from both intra and inter videos). As a result, it outperforms or is on par with most of previous SOTA performance. Note that our framework is independent to the moment-relation modeling network or language encoders, so our DMN could

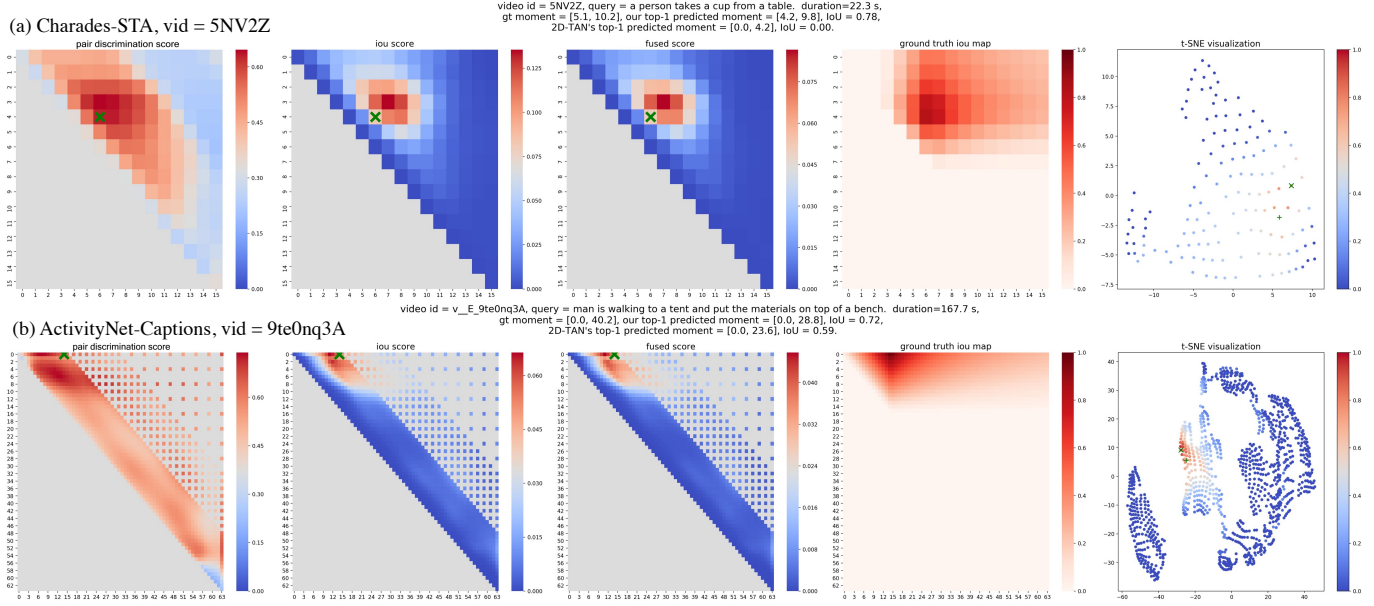


Figure 4. Visualizations on two datasets. Green ‘x’ in the first three maps shows location of GT moment. In the last t-SNE visualization, the matched moment (i.e., has the highest IoU among candidate moments) is a green ‘x’ and the given sentence is a green ‘+’. The colors of unmatched moments shows their IoU with GT moment. We believe the reduced 2D map could help us better understand the results.

Method	R@1		R@5	
	IoU0.5	IoU0.7	IoU0.5	IoU0.7
MCN [23]	17.46	8.01	48.22	26.73
SAP [6]	27.42	13.36	66.37	38.15
SM-RL [67]	24.36	11.17	61.25	32.08
MAN [79]	41.21	20.54	83.21	51.85
DRN [77] [†]	42.90	23.68	87.80	54.87
2D-TAN [82]	39.70	23.31	80.32	51.26
Our DMN	47.31	27.28	<u>83.74</u>	58.41

Table 8. Performance comparison on Charades-STA (VGG feature). [†]our re-production with official code is much lower than the value reported in paper [77].

further boost performance based on a stronger baseline, e.g., MS-2D-TAN [81] with multi-scale modelling capacity. Besides, our computational cost is significantly reduced compared with 2D-TAN [82] due to sharing video features between sentences inside each video. The training process of the baseline takes 36 GPU hours to converge on ActivityNet Captions dataset with RTX-2080Ti, while only 10 GPU hours for ours.

Spatio-temporal video grounding. We also adapt our DMN to spatio-temporally localize tubes that match the given query. This task is recently introduced by Tang *et al.* [59]. We adopt a two-stage method for this task: we first detect human bounding boxes by Faster R-CNN [48] and link them to be candidate tubes following ACT [27]; then, we use our DMN to temporally refine the candidate tubes (see appendix A.5.2 for details). As shown in Tab. 9, our DMN shows significant performance gap over 2D-TAN [82] on the same candidate tubes generated from stage 1. Our method also outperforms some powerful op-

Method	m_vIoU	vIoU@0.3	vIoU@0.5
2D-TAN [82] + WSSTG [8] [†]	15.43	19.83	6.81
STGVT [59] [†]	18.15	26.81	9.48
Yu <i>et al.</i> [74]	30.02	-	-
Tan <i>et al.</i> [57] [‡]	30.40	50.40	18.80
Our stage-1 + 2D-TAN [82]	22.83	36.07	16.96
Our stage-1 + DMN	30.32	49.02	25.56

Table 9. Performance comparison on HC-STVG val set. [†]use smaller train/val set, the values are reported in [59]. [‡]uses an ensemble of 10 models, so it cannot directly compare to ours.

ponents [74, 57] which use strong pre-training models (e.g., LXMERT [58] or MDETR [28]) and ranks first in the STVG challenge of PIC workshop⁴. In contrast, cross-modal interaction modeling in our method is solely achieved by our DMN and no multi-modal pre-training model is used.

Visualizations. In Fig. 4, we show the visualizations in test set on two datasets. Invalid regions of the first three maps are manually set to be in color ‘grey’. Due to highly unbalanced pos./neg. samples of BCE loss in 2D-TAN [82], the absolute value of top-1 result is lower than our expectation. Yet, the gap between top-1 prediction and backgrounds is still discriminative for localizing moments. We conclude that IoU scores tend to be sharp near the GT location yet could be wrong in many situations, while pair discrimination scores tend to cover the right location yet are not sharp among hard negatives. These two score maps are complementary to each other. In our DMN, IoU regression branch is already improved by sharing the same backbone enhanced by pair discrimination loss. However, the perfor-

⁴<http://www.picdataset.com/challenge/task/hcvg>

mance can be further improved a bit (about 0.5%) by fusing their scores with a simple product in our experiments. In the last map, we use t-SNE [63] to visualize features in the joint space ($d^H=256$) to a 2D image. Based on the distribution of moments, we believe our joint space has learn an effective metric for the video and language modalities.

5. Conclusion

In this paper, we propose the Dual Matching Network in the metric learning prospective for temporal grounding in a late-fusion manner. Particularly, we first propose to use the auxiliary task of *dual matching* which asks the model to select the correct sentence in a constructed negative sentence set for video moments in addition to ranking moments given the query sentence. By leveraging the powerful textual negatives, more discriminative features for both modalities are learnt by cross-modal pair discrimination. Moreover, inter-video negatives in temporal grounding is effectively exploited for the first time in our method. With this framework, we achieve state-of-the-art performance on four challenging video grounding benchmarks: Charades-STA, TACoS, ActivityNet-Captions, and HC-STVG.

Acknowledgements. This work is supported by the National Science Foundation of China (No. 62076119, No. 61921006), Program for Innovative Talents and Entrepreneur in Jiangsu Province, and Collaborative Innovation Center of Novel Software Technology and Industrialization. The authors want to thank Yixuan Li for her effort in the spatio-temporal video grounding challenge.

References

- [1] Lei Jimmy Ba, Jamie Ryan Kiros, and Geoffrey E. Hinton. Layer normalization. *CoRR*, abs/1607.06450, 2016. 4
- [2] João Carreira and Andrew Zisserman. Quo vadis, action recognition? A new model and the kinetics dataset. In *CVPR*, 2017. 14, 16
- [3] Jingyuan Chen, Xinpeng Chen, Lin Ma, Zequn Jie, and Tat-Seng Chua. Temporally grounding natural sentence in video. In *EMNLP*, 2018. 2, 3
- [4] Long Chen, Chujie Lu, Siliang Tang, Jun Xiao, Dong Zhang, Chilie Tan, and Xiaolin Li. Rethinking the bottom-up framework for query-based video localization. In *AAAI*, 2020. 2
- [5] Shaoxiang Chen, Wenhao Jiang, Wei Liu, and Yu-Gang Jiang. Learning modality interaction for temporal sentence localization and event captioning in videos. In *ECCV*, 2020. 7
- [6] Shaoxiang Chen and Yu-Gang Jiang. Semantic proposal for activity localization in videos via sentence query. In *AAAI*, 2019. 8
- [7] Ting Chen, Simon Kornblith, Mohammad Norouzi, and Geoffrey E. Hinton. A simple framework for contrastive learning of visual representations. In *ICML*, volume 119 of *Proceedings of Machine Learning Research*, 2020. 3
- [8] Zhenfang Chen, Lin Ma, Wenhan Luo, and Kwan-Yee Kenneth Wong. Weakly-supervised spatio-temporally grounding natural sentence in video. In *ACL (1)*, 2019. 8
- [9] Jia Deng, Wei Dong, Richard Socher, Li-Jia Li, Kai Li, and Fei-Fei Li. Imagenet: A large-scale hierarchical image database. In *CVPR*, 2009. 14
- [10] Jacob Devlin, Ming-Wei Chang, Kenton Lee, and Kristina Toutanova. BERT: pre-training of deep bidirectional transformers for language understanding. In *NAACL-HLT (1)*, 2019. 7, 14, 15, 16
- [11] Christoph Feichtenhofer, Haoqi Fan, Jitendra Malik, and Kaiming He. Slowfast networks for video recognition. In *ICCV*, 2019. 1, 14
- [12] Jiyang Gao, Chen Sun, Zhenheng Yang, and Ram Nevatia. TALL: temporal activity localization via language query. In *ICCV*, 2017. 1, 2, 5, 6, 7
- [13] Jiyang Gao, Zhenheng Yang, Chen Sun, Kan Chen, and Ram Nevatia. TURN TAP: temporal unit regression network for temporal action proposals. In *ICCV*, 2017. 7
- [14] Runzhou Ge, Jiyang Gao, Kan Chen, and Ram Nevatia. MAC: mining activity concepts for language-based temporal localization. In *WACV*, 2019. 2
- [15] Deepthi Ghadiyaram, Du Tran, and Dhruv Mahajan. Large-scale weakly-supervised pre-training for video action recognition. In *CVPR*, 2019. 14
- [16] Soham Ghosh, Anuva Agarwal, Zarana Parekh, and Alexander G. Hauptmann. Excl: Extractive clip localization using natural language descriptions. In *NAACL-HLT (1)*, 2019. 1, 2, 16
- [17] Chunhui Gu, Chen Sun, David A. Ross, Carl Vondrick, Caroline Pantofaru, Yeqing Li, Sudheendra Vijayanarasimhan, George Toderici, Susanna Ricco, Rahul Sukthankar, Cordelia Schmid, and Jitendra Malik. AVA: A video dataset of spatio-temporally localized atomic visual actions. In *CVPR*, 2018. 6
- [18] Raia Hadsell, Sumit Chopra, and Yann LeCun. Dimensionality reduction by learning an invariant mapping. In *CVPR (2)*, 2006. 3
- [19] Dongliang He, Xiang Zhao, Jizhou Huang, Fu Li, Xiao Liu, and Shilei Wen. Read, watch, and move: Reinforcement learning for temporally grounding natural language descriptions in videos. In *AAAI*, 2019. 1, 2
- [20] Kaiming He, Haoqi Fan, Yuxin Wu, Saining Xie, and Ross B. Girshick. Momentum contrast for unsupervised visual representation learning. In *CVPR*, 2020. 3
- [21] Kaiming He, Xiangyu Zhang, Shaoqing Ren, and Jian Sun. Deep residual learning for image recognition. In *CVPR*, 2016. 16
- [22] Fabian Caba Heilbron, Victor Escorcia, Bernard Ghanem, and Juan Carlos Niebles. Activitynet: A large-scale video benchmark for human activity understanding. In *CVPR*, 2015. 5
- [23] Lisa Anne Hendricks, Oliver Wang, Eli Shechtman, Josef Sivic, Trevor Darrell, and Bryan C. Russell. Localizing moments in video with natural language. In *ICCV*, 2017. 1, 2, 5, 7, 8

[24] R. Devon Hjelm, Alex Fedorov, Samuel Lavoie-Marchildon, Karan Grewal, Philip Bachman, Adam Trischler, and Yoshua Bengio. Learning deep representations by mutual information estimation and maximization. In *ICLR*, 2019. 3

[25] Sepp Hochreiter and Jürgen Schmidhuber. Long short-term memory. *Neural Comput.*, 9(8), 1997. 3

[26] Bin Jiang, Xin Huang, Chao Yang, and Junsong Yuan. Cross-modal video moment retrieval with spatial and language-temporal attention. In *ICMR*, 2019. 7

[27] Vicky Kalogeiton, Philippe Weinzaepfel, Vittorio Ferrari, and Cordelia Schmid. Action tubelet detector for spatio-temporal action localization. In *ICCV*, 2017. 3, 8, 14

[28] Aishwarya Kamath, Mannat Singh, Yann LeCun, Ishan Misra, Gabriel Synnaeve, and Nicolas Carion. MDETR - modulated detection for end-to-end multi-modal understanding. *CoRR*, abs/2104.12763, 2021. 8

[29] Prannay Khosla, Piotr Teterwak, Chen Wang, Aaron Sarna, Yonglong Tian, Phillip Isola, Aaron Maschinot, Ce Liu, and Dilip Krishnan. Supervised contrastive learning. In *NeurIPS*, 2020. 3

[30] Ranjay Krishna, Kenji Hata, Frederic Ren, Li Fei-Fei, and Juan Carlos Niebles. Dense-captioning events in videos. In *ICCV*, 2017. 5

[31] Tianhao Li and Limin Wang. Learning spatiotemporal features via video and text pair discrimination. *CoRR*, abs/2001.05691, 2020. 2, 3

[32] Yixuan Li, Zixu Wang, Limin Wang, and Gangshan Wu. Actions as moving points. In *ECCV*, 2020. 1, 3

[33] Tsung-Yi Lin, Piotr Dollár, Ross B. Girshick, Kaiming He, Bharath Hariharan, and Serge J. Belongie. Feature pyramid networks for object detection. In *CVPR*, 2017. 14

[34] Tianwei Lin, Xiao Liu, Xin Li, Errui Ding, and Shilei Wen. BMN: boundary-matching network for temporal action proposal generation. In *ICCV*, 2019. 1

[35] Tsung-Yi Lin, Michael Maire, Serge J. Belongie, James Hays, Pietro Perona, Deva Ramanan, Piotr Dollár, and C. Lawrence Zitnick. Microsoft COCO: common objects in context. In *ECCV* (5), volume 8693 of *Lecture Notes in Computer Science*, 2014. 14

[36] Tianwei Lin, Xu Zhao, Haisheng Su, Chongjing Wang, and Ming Yang. BSN: boundary sensitive network for temporal action proposal generation. In *ECCV*, 2018. 1

[37] Zhijie Lin, Zhou Zhao, Zhu Zhang, Zijian Zhang, and Deng Cai. Moment retrieval via cross-modal interaction networks with query reconstruction. *IEEE Trans. Image Process.*, 29, 2020. 3, 7

[38] Bingbin Liu, Serena Yeung, Edward Chou, De-An Huang, Li Fei-Fei, and Juan Carlos Niebles. Temporal modular networks for retrieving complex compositional activities in videos. In *ECCV*, 2018. 2, 7

[39] Ilya Loshchilov and Frank Hutter. Decoupled weight decay regularization. In *ICLR*, 2019. 12, 15

[40] Chuju Lu, Long Chen, Chilie Tan, Xiaolin Li, and Jun Xiao. DEBUG: A dense bottom-up grounding approach for natural language video localization. In *EMNLP/IJCNLP* (1), 2019. 1, 2, 3

[41] Antoine Miech, Jean-Baptiste Alayrac, Lucas Smaira, Ivan Laptev, Josef Sivic, and Andrew Zisserman. End-to-end learning of visual representations from uncurated instructional videos. In *CVPR*, 2020. 3

[42] Jonghwan Mun, Minsu Cho, and Bohyung Han. Local-global video-text interactions for temporal grounding. In *CVPR*, 2020. 2, 3, 7, 16

[43] Cristian Rodriguez Opazo, Edison Marrese-Taylor, Fatehmeh Sadat Saleh, Hongdong Li, and Stephen Gould. Proposal-free temporal moment localization of a natural-language query in video using guided attention. In *WACV*, 2020. 2, 3, 16

[44] Mayu Otani, Yuta Nakashima, Esa Rahtu, and Janne Heikkilä. Uncovering hidden challenges in query-based video moment retrieval. In *BMVC*, 2020. 4, 7

[45] Jeffrey Pennington, Richard Socher, and Christopher D. Manning. Glove: Global vectors for word representation. In *EMNLP*, 2014. 3, 15

[46] Vasili Ramanishka, Abir Das, Jianming Zhang, and Kate Saenko. Top-down visual saliency guided by captions. In *CVPR*, 2017. 3

[47] Michaela Regneri, Marcus Rohrbach, Dominikus Wetzel, Stefan Thater, Bernt Schiele, and Manfred Pinkal. Grounding action descriptions in videos. *Trans. Assoc. Comput. Linguistics*, 1, 2013. 5

[48] Shaoqing Ren, Kaiming He, Ross B. Girshick, and Jian Sun. Faster R-CNN: towards real-time object detection with region proposal networks. In *NIPS*, 2015. 8

[49] Anna Rohrbach, Marcus Rohrbach, Ronghang Hu, Trevor Darrell, and Bernt Schiele. Grounding of textual phrases in images by reconstruction. In *ECCV*, 2016. 3

[50] Marcus Rohrbach, Michaela Regneri, Mykhaylo Andriluka, Sikandar Amin, Manfred Pinkal, and Bernt Schiele. Script data for attribute-based recognition of composite activities. In *ECCV*, 2012. 5

[51] Victor Sanh, Lysandre Debut, Julien Chaumond, and Thomas Wolf. Distilbert, a distilled version of BERT: smaller, faster, cheaper and lighter. *CoRR*, abs/1910.01108, 2019. 3, 6, 12, 16

[52] Gunnar A. Sigurdsson, Gülcin Varol, Xiaolong Wang, Ali Farhadi, Ivan Laptev, and Abhinav Gupta. Hollywood in homes: Crowdsourcing data collection for activity understanding. In *ECCV*, 2016. 5

[53] Karen Simonyan and Andrew Zisserman. Very deep convolutional networks for large-scale image recognition. In *ICLR*, 2015. 12

[54] Kihyuk Sohn. Improved deep metric learning with multi-class n-pair loss objective. In *NIPS*, 2016. 3

[55] Yi Sun, Xiaogang Wang, and Xiaoou Tang. Deep learning face representation from predicting 10,000 classes. In *CVPR*, 2014. 3

[56] Christian Szegedy, Wei Liu, Yangqing Jia, Pierre Sermanet, Scott E. Reed, Dragomir Anguelov, Dumitru Erhan, Vincent Vanhoucke, and Andrew Rabinovich. Going deeper with convolutions. In *CVPR*, 2015. 16

[57] Chaolei Tan, Zihang Lin, Jianfang Hu, Xiang Li, and Wei-Shi Zheng. Augmented 2d-tan: A two-stage approach

for human-centric spatio-temporal video grounding. *CoRR*, abs/2106.10634, 2021. 8

[58] Hao Tan and Mohit Bansal. LXMERT: learning cross-modality encoder representations from transformers. In *EMNLP/IJCNLP (1)*, 2019. 8

[59] Zongheng Tang, Yue Liao, Si Liu, Guanbin Li, Xiaojie Jin, Hongxu Jiang, Qian Yu, and Dong Xu. Human-centric spatio-temporal video grounding with visual transformers. *CoRR*, abs/2011.05049, 2020. 1, 3, 6, 8, 14

[60] Du Tran, Lubomir D. Bourdev, Rob Fergus, Lorenzo Torresani, and Manohar Paluri. Learning spatiotemporal features with 3d convolutional networks. In *ICCV*, 2015. 12

[61] Du Tran, Heng Wang, Matt Feiszli, and Lorenzo Torresani. Video classification with channel-separated convolutional networks. In *ICCV*, 2019. 14

[62] Aäron van den Oord, Yazhe Li, and Oriol Vinyals. Representation learning with contrastive predictive coding. *CoRR*, abs/1807.03748, 2018. 3

[63] Laurens van der Maaten and Geoffrey Hinton. Visualizing data using t-sne. *Journal of Machine Learning Research*, 9(86), 2008. 9

[64] Jingwen Wang, Lin Ma, and Wenhao Jiang. Temporally grounding language queries in videos by contextual boundary-aware prediction. In *AAAI*, 2020. 2, 3

[65] Limin Wang, Wei Li, Wen Li, and Luc Van Gool. Appearance-and-relation networks for video classification. In *CVPR*, 2018. 1

[66] Limin Wang, Yuanjun Xiong, Zhe Wang, Yu Qiao, Dahua Lin, Xiaoou Tang, and Luc Van Gool. Temporal segment networks: Towards good practices for deep action recognition. In *ECCV*, 2016. 1

[67] Weining Wang, Yan Huang, and Liang Wang. Language-driven temporal activity localization: A semantic matching reinforcement learning model. In *CVPR*, 2019. 2, 7, 8

[68] Thomas Wolf, Lysandre Debut, Victor Sanh, Julien Chaumond, Clement Delangue, Anthony Moi, Pierrick Cistac, Tim Rault, Rémi Louf, Morgan Funtowicz, and Jamie Brew. Huggingface’s transformers: State-of-the-art natural language processing. *CoRR*, abs/1910.03771, 2019. 12, 15, 16

[69] Jie Wu, Guanbin Li, Si Liu, and Liang Lin. Tree-structured policy based progressive reinforcement learning for temporally language grounding in video. In *AAAI*, 2020. 2

[70] Zhirong Wu, Yuanjun Xiong, Stella X. Yu, and Dahua Lin. Unsupervised feature learning via non-parametric instance discrimination. In *CVPR*, 2018. 3

[71] Saining Xie, Ross B. Girshick, Piotr Dollár, Zhuowen Tu, and Kaiming He. Aggregated residual transformations for deep neural networks. In *CVPR*, 2017. 14

[72] Huijuan Xu, Kun He, Bryan A. Plummer, Leonid Sigal, Stan Sclaroff, and Kate Saenko. Multilevel language and vision integration for text-to-clip retrieval. In *AAAI*, 2019. 2, 3, 7

[73] Mengmeng Xu, Chen Zhao, David S. Rojas, Ali K. Thabet, and Bernard Ghanem. G-TAD: sub-graph localization for temporal action detection. In *CVPR*, 2020. 1

[74] Yi Yu, Xinying Wang, Wei Hu, Xun Luo, and Cheng Li. 2rd place solutions in the HC-STVG track of person in context challenge 2021. *CoRR*, abs/2106.07166, 2021. 8

[75] Yitian Yuan, Lin Ma, Jingwen Wang, Wei Liu, and Wenwu Zhu. Semantic conditioned dynamic modulation for temporal sentence grounding in videos. In *NeurIPS*, 2019. 1, 2, 3, 7, 16

[76] Yitian Yuan, Tao Mei, and Wenwu Zhu. To find where you talk: Temporal sentence localization in video with attention based location regression. In *AAAI*, 2019. 2, 7

[77] Runhao Zeng, Haoming Xu, Wenbing Huang, Peihao Chen, Mingkui Tan, and Chuang Gan. Dense regression network for video grounding. In *CVPR*, 2020. 1, 2, 3, 7, 8, 15, 16

[78] Binjie Zhang, Yu Li, Chun Yuan, Dejing Xu, Pin Jiang, and Ying Shan. A simple yet effective method for video temporal grounding with cross-modality attention. *CoRR*, abs/2009.11232, 2020. 3

[79] Da Zhang, Xiyang Dai, Xin Wang, Yuan-Fang Wang, and Larry S. Davis. MAN: moment alignment network for natural language moment retrieval via iterative graph adjustment. In *CVPR*, 2019. 1, 2, 3, 8

[80] Hao Zhang, Aixin Sun, Wei Jing, and Joey Tianyi Zhou. Span-based localizing network for natural language video localization. In *ACL*, 2020. 2

[81] Songyang Zhang, Houwen Peng, Jianlong Fu, Yijuan Lu, and Jiebo Luo. Multi-scale 2d temporal adjacent networks for moment localization with natural language. *CoRR*, abs/2012.02646, 2020. 8

[82] Songyang Zhang, Houwen Peng, Jianlong Fu, and Jiebo Luo. Learning 2d temporal adjacent networks for moment localization with natural language. In *AAAI*, 2020. 1, 2, 3, 4, 5, 6, 7, 8, 12, 13, 15, 16

[83] Yue Zhao, Yuanjun Xiong, Limin Wang, Zhirong Wu, Xiaoou Tang, and Dahua Lin. Temporal action detection with structured segment networks. In *ICCV*, 2017. 1

Appendix

A Additional Details

A.1. Sparse 2D Feature Map in 2D-TAN

To save the effort for readers to read the original paper, we adapt some descriptions in the 2D-TAN paper [82] about the sparse 2d moment map here to show some important details. In our paper, we directly use this sparse strategy to construct our feature map without any adaptation. The details of sparse 2D feature map is as follows.

The 2D temporal feature map \mathbf{F}^M consists of three dimensions: the first two dimensions N represent the start and end clip indexes respectively, while the third one d^V indicates the feature dimension. The feature of a moment starting from clip v_a to v_b is located at $\mathbf{F}^M[a, b, :]$ on the feature map, where $\mathbf{F}^M[a, b, :] = \mathbf{f}_{a,b}^M$. Noted that, the moment's start and end clip indexes a and b should satisfy $a \leq b$. Therefore, on the 2D temporal feature map, all the moment candidates locating at the region of $a > b$ are invalid, i.e. the lower triangular part of the map, as shown in Figure 5. The values in this region are padded with zeros in implementation.

The previous three steps introduce the feature extraction of moments, but do not specify how to select possible moments as candidates. One simple way is to enumerate all the possible consecutive video clips as candidates. However, this strategy will bring much computational cost to subsequent moment-sentence matching and retrieval. Therefore, we propose a sparse sampling strategy, as shown in Figure 5. The key idea is to remove the redundant moments which have large overlaps with the selected candidates.

Specifically, we densely sample moments of short duration, and gradually increase the sampling interval when the moment duration becomes long. In more details, when the number of sampled clips is small, i.e. $N \leq 16$, we enumerate all possible moments as candidates. When N becomes large, i.e. $N > 16$, a moment starting from clip v_a to v_b is selected as the candidate when satisfying the following condition $G(a, b)$:

$$G(a, b) \Leftarrow (a \bmod s=0) \& ((b - s') \bmod s=0), \quad (9)$$

where a and b are the indexes of clips, s and s' are defined as:

$$s = 2^{k-1},$$

$$s' = \begin{cases} 0 & \text{if } k = 1, \\ 2^{k+2} - 1 & \text{otherwise.} \end{cases} \quad (10)$$

Here, $k = \lceil \log_2(\frac{b-a+1}{8}) \rceil$, and $\lceil \cdot \rceil$ is the ceil function. If $G(a, b) = 1$, the moment is selected as the candidate, otherwise, it is not selected. This sampling strategy can largely reduce the number of moment candidates, as well as the computational cost.

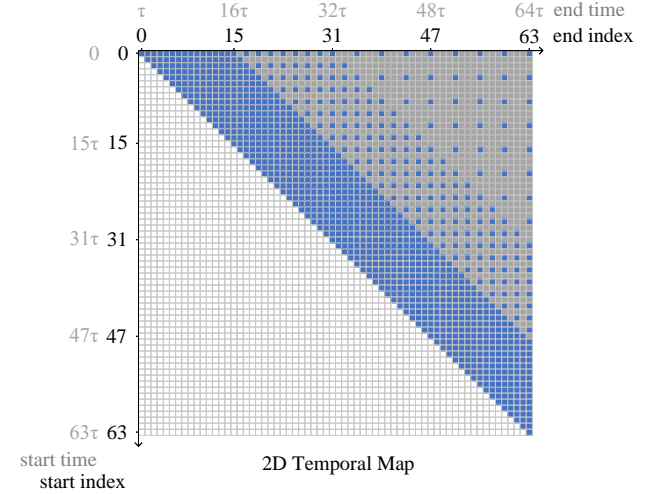


Figure 5. The selection of moment candidates when there are $N = 64$ sampled clips in an untrimmed video. The upper triangular part of the 2D map enumerates all possible moment candidates starting from clip v_a to v_b , while the lower triangular part is invalid. In our method, only the *blue* points are selected as moment candidates. Best viewed in color.

A.2. More Implementation Details about DMN

For convolutional networks, we use exactly the same settings with 2D-TAN [82] (max-pool version) for fair comparisons, including visual features (VGG [53] feature for Charades and C3D [60] features for ActivityNet-Captions and TACoS), number of sampled clips N , number of 2D convolution network layers L , kernels K and channels d^V , non maximum suppression (NMS) threshold, scaling thresholds t_{min} and t_{max} . We set the dimension of the joint feature space d^H as 256, temperatures τ_s and τ_v as 0.1. In pair discrimination loss, we only sample negative moments lower than IoU=0.5 and set margin m as 0.1, 0.3 and 0.4 for TACoS, ActivityNet-Captions and Charades-STA respectively. We use the implementation from HuggingFace [68] with the pre-trained model ‘distilbert-base-uncased’ for both DistilBERT [51] model and its tokenzier. We use AdamW [39] optimizer with learning rate of 1×10^{-4} and batch size 48 for Charades, learning rate of 8×10^{-4} and batch size 48 for ActivityNet Captions and learning rate of 1.5×10^{-3} and batch size 4 for TACoS. The learning rate is divided by a factor of 10 every 8 epochs for the first two datasets. We set λ of pair discrimination loss as 0.1 for ActivityNet Captions and 0.05 for Charades and TACoS. We early stop the pair discrimination loss when we observe its performance on validation set starts to drop. The learning rate of DistilBERT is always 1/10 of our main model.

For fusing pair discrimination scores and IoU regression scores, we mentioned that we use the product to fuse scores



Figure 6. Explanations for BERT’s last layer. Credit to this webpage (<https://stackoverflow.com/questions/62705268/why-bert-transformer-uses-cls-token-for-classification-instead-of-average-over>).

in two joint visual-language spaces in our paper:

$$s = s^{iou} \cdot s^c. \quad (11)$$

Actually, the region of $s^{iou} \in (0, 1)$ and $s^c \in (-1, 1)$ can not directly fuse due to the negative regions of s^c . We rescale the s^c as $s_{scaled}^c = (s^c + 1)/2$ and use the product of s_{scaled}^c and s^{iou} to evaluate the moments. In inference, the value of scores are not important yet the ranking order is more important. Therefore, the rescaled s^c will not harm the final performance. The fusion strategy we use in the implementation is

$$s = s^{iou} \cdot s_{scaled}^c = s^{iou} \cdot \frac{s^c + 1}{2}. \quad (12)$$

We use a third-party implementation⁵ of 2D-TAN which is recognized by the authors of 2D-TAN in the official code webpage⁶. The third-party implementation adds the support for *DistributedDataParallel* in Pytorch therefore has the advantage of faster training speed. The performance of 2D-TAN reported in our paper is obtained by the third-party implementation with the official configuration file. The code of DMN is developed on the third-party implementation of 2D-TAN.

A.3. Early-fusion vs. Late-fusion

To the best of our knowledge, the computer vision and multi-media community commonly use two types of modality fusion: early-fusion and late-fusion.

(1) Early-fusion commonly fuses modalities at the first few layers, e.g., concatenate features from different modalities as the fused feature, and then performs heavy computations by neural networks on the fused features. Although the

feature extractors for each modality could be heavy (e.g., video clip feature extractors or optical flow feature extractors), we still regard a method as an early-fusion method if heavy computations for the specific task (e.g., detection/classification) is performed on the fused multi-modal feature. Early-fusion methods often have more flexibility to model the interactions between modalities, yet the computational cost is often larger.

(2) Late-fusion commonly model different modalities independently by different networks and we only fuse the information from different modalities at the last layer. e.g., taking the average of class-wise confidence scores predicted from different modalities as the final prediction in classification model, or taking the cosine similarity of feature vectors of two modalities as the final prediction in our DMN. Late-fusion methods often shows better computational efficiency due to the decoupled modalities. Our metric learning perspective in a late-fusion manner achieves highly competitive performance with the early-fusion baseline in fair comparison (i.e., without pair discrimination loss), yet it uses much lower training cost.

We adopt late-fusion in our method due to two advantages: (1) It enables our dual matching scheme (i.e., adding pair discrimination loss); (2) It shows significant advantages in training cost (36 GPU hours of baseline [82] vs. 10 GPU hours of our DMN in ActivityNet-Captions dataset with RTX-2080Ti.)

A.4. More Information about BERT

In the paper, we mentioned that there are two ways to get the sentence-level feature: (1) use ‘CLS’ token, and (2) use the average pooling of all tokens. To save the time for readers who are not familiar with the BERT-family models, we give some details about this two aggregation strategies.

⁵<https://github.com/ChenJoya/2dtan>

⁶<https://github.com/microsoft/2D-TAN>

In the original BERT [10] paper, they use a special token ‘CLS’ to automatically aggregate the information of whole input sequence by the self-attention operation in the transformer layers. Then, they use the last layer’s feature of ‘CLS’ token to get the sentence-level feature or train a binary classifier for determining whether the total sequence, which may contains several sentences, is coherent upon the feature of ‘CLS’ token. As shown in Fig. 6, the ‘CLS’ token is the first position in each sequence, i.e., if the dimension of the tensor for the last layer of BERT is [Batch, Sequence, Channel], then ‘CLS’ token for the i_{th} sequence is [i, 0, :] (in Python-style, ‘:’ means all elements). The spirit of BERT-family models is to use this token to represent the information of the entire sequence and let the transformers to learn their interactions automatically.

In many computer vision tasks, we often use global average pooling to aggregate information from the spatial or the temporal dimensions. So we also try this way of aggregation in temporal grounding task, i.e., average pooling for the i_{th} sequence is using the average from [i, 1, :] to [i, N, :] (N means the last word token). Our experiment shows average pooling has very few advantages in performance and much faster convergence speed for temporal grounding task, therefore we use it as default in our model.

A.5. More Details about STVG Task

A.5.1 Metrics

Here we adapt some descriptions of metrics in the HC-STVG paper [59] to save readers’ time. The main evaluation metric for HC-STVG is vIoU, and it is defined as follow:

$$vIoU = \frac{1}{|T_{\text{union}}|} \sum_{t \in T_{\text{inter}}} \text{IoU}(B'_t, B_t) \quad (13)$$

where $T_{\text{inter}} = T_p \cap T_{GT}$ refers to the intersected frames between the predicted tube T_p and the ground-truth (GT) tube T_{GT} , $T_{\text{union}} = T_p \cup T_{GT}$ represents the union set of the predicted frames and the GT frames, B'_t and B_t are the predicted bounding box and the ground truth bounding box at frame t . vIoU reflects the accuracy of the predicted spatio-temporal tubes. The **vIoU@perc.** score stands for the percentage of predicted tubes whose vIoU is larger than perc. and m_{vIoU} is the average of vIoUs score over the whole test set. Based on Equation 13, vIoU is approximated by a product of temporal IoU (tIoU) and average of spatial IoU (sIoU).

In our experiments, we use m_{vIoU} , vIoU@0.3 and vIoU@0.5 for comparisons with other methods.

A.5.2 Details of our STVG method

As shown in Fig. 7, a two-stage model is used to tackle the STVG problem: 1) in stage 1, we detect human bounding

boxes in all frames and link them to generate candidate action tubes, then we extract ROI features for each bounding box to capture the motion cues; 2) in stage 2, we use our Dual Matching Network to evaluate the temporal regions of each candidate tube by a 2D moment map, automatically locate the right tube and finally refine the tube temporally.

Tubes Generation and Features Extraction. In the first stage, we detect human bounding boxes in all frames and link them to generate candidate action tubes, then we extract ROI features for each bounding box to capture the motion cues of every candidate action tubes: for human bounding boxes, we use a Faster R-CNN with a ResNeXt-101-FPN [71, 33] backbone, which is pre-trained on ImageNet [19] and the COCO human keypoint images [35]. For linking tubes, we follow the ACT method [27] to link the bounding boxes into candidate tubes. For ROI features, we use ir-CSN-152 [61] pretrained on IG-65M [15] to extract 1024-dimensional RGB features and SlowOnly [11] (4×16) pretrained on Kinetics [2] to extract 1024-d optical flow features. We combine them by concatenation, thus we get a 2048-d feature for a bounding box. To reduce computation, we use step size 2 when extracting ROI features, that is, extracting one feature for every two bounding boxes. For a tube with T frames, we get a $(T/2) \times 2048$ feature.

Temporal Refinement with DMN. We use our DMN to refine the temporal regions of each candidate tube. There are some adaptations to make our temporal grounding feasible for spatio-temporal video grounding: (1) For each video, there are several generated candidate tubes instead of only one feature sequence in temporal grounding. So we generate the same number of 2D moment maps with the candidate tubes. However, the positive moment is selected by the highest vIoU among elements in all 2D moment maps and all the rest moments are negatives. The IoU regression branch also uses the scaled vIoU as the groundtruth. Therefore, we do not need to first select the right candidate tube by a complex evaluation module (e.g., transformer in the baseline of HC-STVG dataset [59]) and then refine the only one predicted tube. Instead, we just use vIoU-based supervisions to automatically let our DMN to find the right tube and the appropriate temporal refinement: as shown in Fig. 8, although the red tube has a high tIoU with the groundtruth tube (green tube), it has a low spatial IoU. Therefore, in our 2D moment maps’ GT, the red tube will be assigned a very low score and regraded as the background region. The dark blue tube with high vIoU will be assigned a high score and therefore automatically selected by our DMN and then perform a temporal refinement to achieve the final result.

Training and Inference. Our models are trained with a batch size of 32 on a server with 8 GPUs. For the final testing submission, we train the model on the combined datasets of training and validation. We freeze the parameters of BERT [10] in the first 5 epochs and then jointly

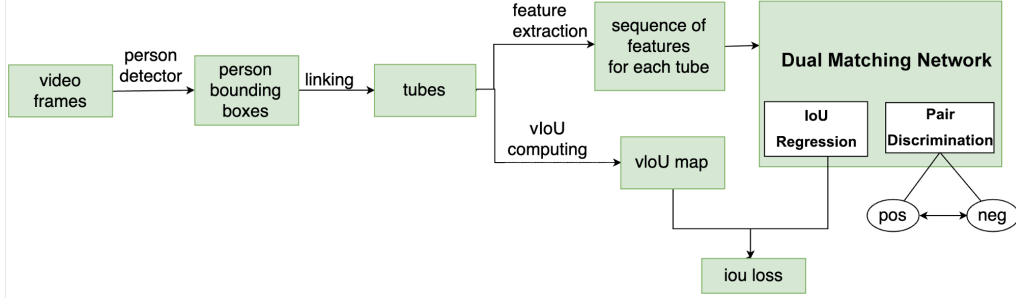


Figure 7. Architecture of our STVG method with DMN.

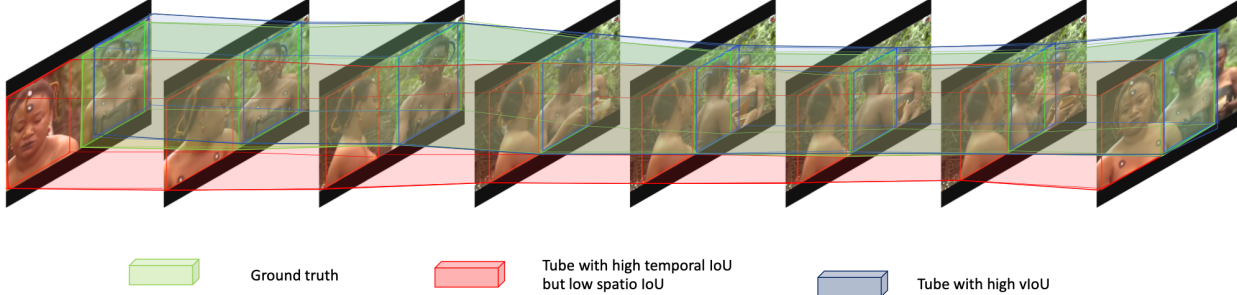


Figure 8. Visualization of how we use vIoU supervision to automatically select the right tube.

train the entire model including BERT [10] for the rest of the epochs. We use both IoU loss and pair discrimination loss in the first 7 epochs, and then we only use IoU loss to make the model converge. We train all models for 20 epochs. We use AdamW [39] optimizer, and a learning rate of 1e-4 where we use a 1/10 learning rate (i.e., 1e-5) to finetune the pretrained BERT [10] model. The learning rates for all parts of our model will be decreased by a factor of 10 at epoch 9 and 16.

We use the product of the predicted IoU score and the pair discrimination score as the final confidence score of a tube proposal. We choose the tube proposal with the highest score as the predicted top-1 result. Then three vIoU-based metrics are computed on this top-1 tube prediction.

B More Experiments

B.1. Impact of DistilBERT

As shown in Tab. 10, we construct two baselines with DistilBERT, which are DRN [77] and 2D-TAN [82]. We can observe that the usage of DistilBERT has very little impact to the final performance in both methods. Therefore, we believe our comparison with previous SOTA methods is fair. The reason of our usage of DistilBERT in our DMN is to call for standardization: we observe that the usage of LSTM involves different GloVe [45] embeddings, different LSTM layers or if it is bi-directional, which may lead to notable gap in performance. As for DistilBERT, the performance can be fairly compared by loading the same pre-

Charades-STA	Feature	R@1		R@5	
		IoU0.5	IoU0.7	IoU0.5	IoU0.7
DRN [†] [77]	C3D	<i>43.26</i>	23.95	85.43	52.82
DRN w/ DistilBERT	C3D	42.62	23.50	<i>85.84</i>	<i>53.59</i>
2D-TAN [82]	VGG	39.70	23.31	80.32	51.26
2D-TAN [†]	VGG	40.03	23.15	<i>82.18</i>	49.89
2D-TAN w/ DistilBERT	VGG	<u>40.32</u>	<u>23.81</u>	79.49	51.96

Table 10. The impact of DistilBERT. (top) DRN w/ LSTM vs. DRN w/ DistilBERT. The best result of DRN [77] is highlighted by *italic* font. (bottom) 2D-TAN w/ LSTM vs. 2D-TAN w/ DistilBERT. The best results are highlighted by underlines. [†] means our implementation.

trained model in HuggingFace transformers [68]. We will explain the unfair comparison of LSTM in details in B.2.

Training Details. Similar to our training strategy of DistilBERT, we freeze it for the first several epochs and finetune it with learning rate as 1/10 of other parts in the DistilBERT version of DRN and 2D-TAN. The number of frozen epochs depends on when the performance on validation set starts to increase slowly or even drop. Then, we will allow the back-propagated gradients in DistilBERT to finetune it in our dataset. The factor of 1/10 is an empirical value in our experiments due to the quick over-fitting if use the same learning rate with our convolution model.

B.2. LSTM

B.2.1 Unfair comparisons of LSTM.

We observe unfair comparisons of LSTM in previous methods: The released GloVe [45] embeddings have several

Language Models	R@1		R@5	
	IoU0.5	IoU0.7	IoU0.5	IoU0.7
GloVe (6B)	39.70	23.31	80.32	51.26
GloVe (6B) [†]	40.03	23.15	82.18	49.89
GloVe (840B)	39.83	23.44	79.68	54.14
DistilBERT	40.32	23.81	79.49	51.96

Table 11. Comparisons between different language models in 2D-TAN [82] model on Charades-STA dataset, including different pre-trained GloVe embeddings and DistilBERT model. [†] means our implementation of 2D-TAN with GloVe 6B.

types: 6B on wikipedia, 42B and 840B on Common Crawl, and 27B on Twitter. The inconsistent setting of pre-trained GloVe word embedding among previous works make the performance unfair to compare. For example, 2D-TAN [82] use the 6B version and SCDM [75] use the 840B version. DRN [77] claims it uses a GloVe pre-trained model in the paper, but in the released code⁷ it uses an embedding layer with a pre-defined dictionary and the performance in the paper is impossible to reproduce. We try to reproduce the performance strictly following the directions in the official code, yet the performance is about 2% worse than the reported result (see Tab. 10 for our reproduced result). In Tab. 11, we compare the performance of 2D-TAN with different language models, including different pre-trained GloVe embeddings and the DistilBERT model. The 840B version of GloVe model has a notable performance gain in R@5(IoU=0.7) and similar performance with other models in other metrics.

Based on the above concerns, we choose DistilBERT [51] with the pre-trained model from HuggingFace [68] and hope that more attention could be paid to fair comparisons. DistilBERT is a light-weight version of BERT [10] and only contains 66M parameters. We conduct experiments of baseline with DistilBERT and compare our result with the baseline fairly. More details about our usage of DistilBERT will be explained below.

B.2.2 Our DMN with LSTM.

Due to the Siamese-alike network architecture of our method, the model capacity of two encoders for each modality should be approximately equal, otherwise the one with less capacity will overfit in the training process easily. Based on this concern, we adopt DistilBERT for a balanced model capacity with convolution network. Although the encoders for language queries in our DMN can be replaced by any other language models and it is not our contribution or focus in our framework, it does influence the final temporal grounding performance. In Tab. 12, we ablate the impact of different language encoders in our framework. The effectiveness of our framework can be supported by the performance gap between only using BCE loss (the same super-

⁷<https://github.com/Alvin-Zeng/DRN>

Language Models	R@1		R@5	
	IoU0.5	IoU0.7	IoU0.5	IoU0.7
DistilBERT w/ BCE loss	40.12	23.89	79.57	53.26
DistilBERT w/ both losses*	47.31	27.28	83.74	58.41
Performance gap	7.19	3.39	4.17	5.15
LSTM w/ BCE loss	38.20	22.31	78.84	52.76
LSTM w/ both losses	42.42	26.40	83.39	59.89
Performance gap	4.22	4.09	4.55	7.13

Table 12. Comparisons between different language models in our proposed DMN on Charades-STA dataset. * the version we used as DMN’s final performance.

vision signals with 2D-TAN [82]) and using both BCE and pair discrimination loss. By adding new supervision signals (i.e., pair discrimination loss), the performance gap of DistilBERT is even smaller than the gap of LSTM except the metric R@1(IoU=0.5). This result shows the effectiveness of our framework regardless the used language encoders.

Besides, we guess the reason of worse performance of LSTM w/ BCE loss in Tab. 12 compared to the baseline 2D-TAN [82] is the unbalanced model capacity in our Siamese-alike late-fusion architecture, while 2D-TAN [82] uses the early-fusion strategy and the heavy convolution network operates on the fused features.

B.3. I3D Feature

As for I3D feature on the Charades-STA dataset, the problem of unfair comparisons is even more serious. For example, ExCL [16], TMLGA [43] and LGI [42] use RGB-only I3D [2] feature with Inception [56] backbone, while DRN [77] uses two-stream I3D feature with ResNet-50 [21] backbone⁸, leading to a significant difference of performance by the feature itself. Our implementation of DRN with the same I3D feature with ExCL, TMLGA and LGI achieves much worse performance than the reported result in the original DRN paper (larger than 6% in R@1). We also show the difference in Tab. 13. Consider that a huge performance gap will be made simply due to the different inputs (RGB-only vs. two-stream) or backbones (Inception in original I3D paper [2] vs. other variants with stronger backbone like ResNet-50), we hope that the usage of I3D feature on Charades-STA dataset could be reduced for fair comparisons.

B.4. Performance Comparisons by Moment Length

To further discover our model’s improvement over the baseline [82], we decompose the performance comparisons by the proportion of moment’s length in the whole video. Fig. 9-12 contain comparisons under different metrics on

⁸The official code does not release the I3D feature for reproduction. We guess the I3D feature is two-stream with ResNet-50 backbone based on the configuration file: the filename of I3D feature is ‘I3d_resnet50_unit64_overlap0.875_merged’ and the feature dimension is 2048, where commonly RGB-only I3D feature’s dimension is 1024 while two-stream’s is 2048.

13D feature	R@1		R@5	
	IoU0.5	IoU0.7	IoU0.5	IoU0.7
RGB-only, Inception-v1 [†]	47.61	25.46	85.11	52.37
Two-stream, ResNet-50	53.09	31.75	89.06	60.05

Table 13. Comparisons between different 13D features in DRN on Charades-STA dataset. [†] means our implementation.

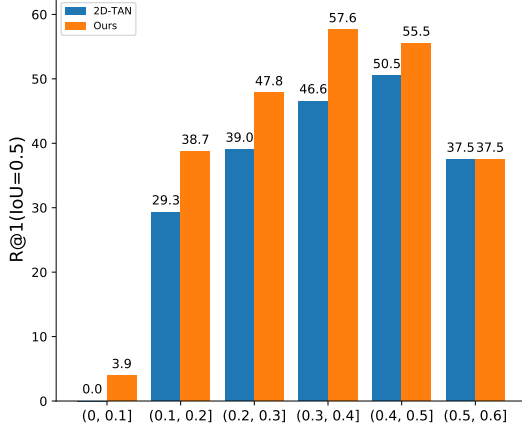


Figure 9. Comparisons of R@1(IoU=0.5) on Charades-STA.

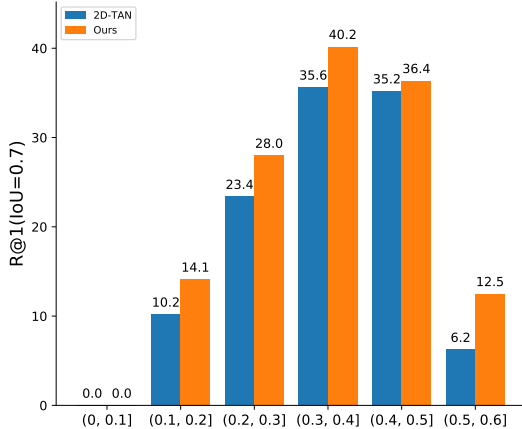


Figure 10. Comparisons of R@1(IoU=0.7) on Charades-STA.

Charades-STA dataset. The x-axis is grouped by the proportion of moment's length in the whole video. The x-axis stops in 0.6 due to the maximum length on Charades-STA dataset is less than 0.6. It is worth noticing that the intervals of proportion is not balanced, therefore some intervals may have huge difference due to the small total number. In our statistics, the number of ground truth moments in these intervals are 51, 1020, 1347, 769, 517, 16 from (0, 0.1] to (0.5, 0.6]. The comparisons on Charades-STA dataset vary a lot in different metrics. The main parts of improvement for R@1 are obtained in middle lengths (0.2 to 0.4), yet the one for R@5 are in small lengths (0 to 0.2). The performances with IoU=0.5 are more likely to saturate, especially in longer lengths, while IoU=0.7 tends to be improved in all

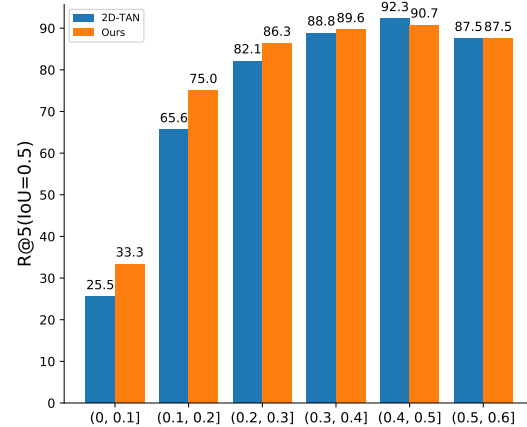


Figure 11. Comparisons of R@5(IoU=0.5) on Charades-STA.

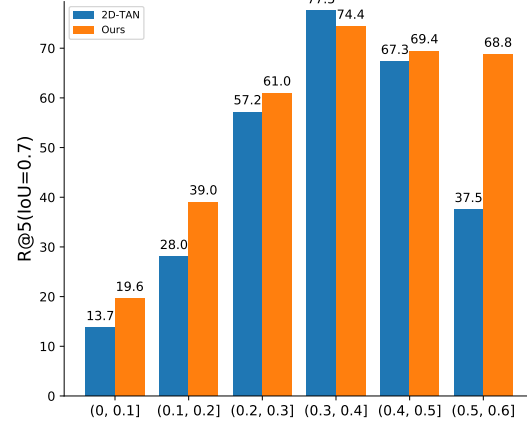


Figure 12. Comparisons of R@5(IoU=0.7) on Charades-STA.

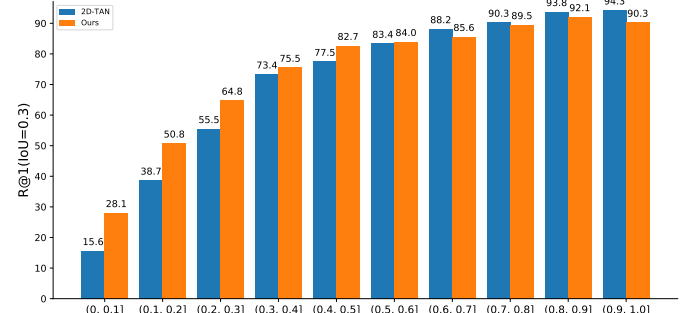


Figure 13. Comparisons of R@1(IoU=0.3) on ActivityNet-Captions.

lengths.

We also conduct the similar experiments in ActivityNet-Captions dataset, which is shown in Fig. 13-18. Here all the intervals have many instances, indicating the longer duration in ActivityNet Captions dataset. The number of ground truth moments in these intervals are 2966, 3152,

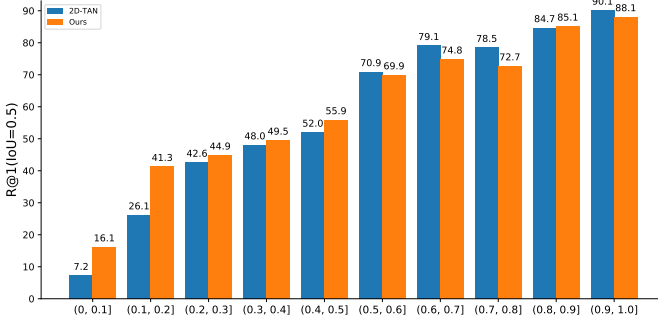


Figure 14. Comparisons of R@1(IoU=0.5) on ActivityNet-Captions.

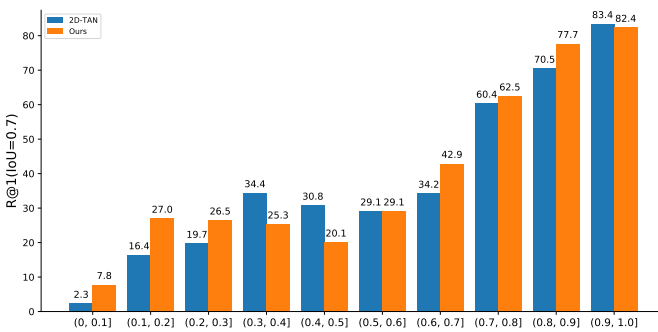


Figure 15. Comparisons of R@1(IoU=0.7) on ActivityNet-Captions.

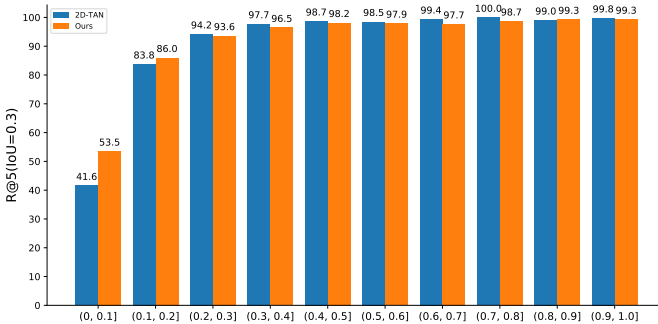


Figure 16. Comparisons of R@5(IoU=0.3) on ActivityNet-Captions.

2738, 2515, 2056, 1017, 473, 381, 417, 1316 from (0, 0.1] to (0.9, 1.0]. Although our model shares the similar visual modeling backbone with 2D-TAN, the performance of our model due to the auxiliary dual matching task by pair discrimination differs from the baseline a lot. Specifically, we achieve a much better performance in short moments yet similar performance with 2D-TAN in long moments. Our performance of long moments suffers even more in R@5, indicating that our discriminative features lead to a sharper prediction where all top-5 predictions are in the similar regions if the NMS threshold is not appropriately adjusted.

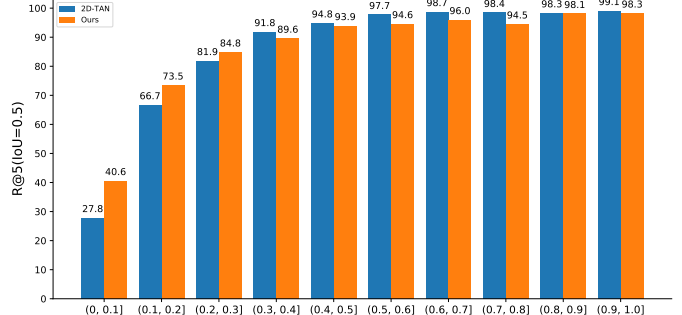


Figure 17. Comparisons of R@5(IoU=0.5) on ActivityNet-Captions.

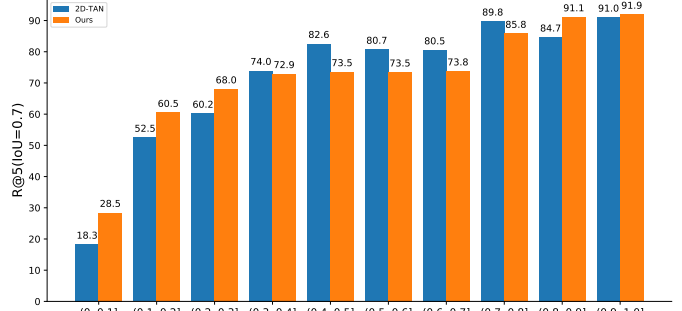


Figure 18. Comparisons of R@5(IoU=0.7) on ActivityNet-Captions.

We want to raise the attention of readers that much more moments are in the short regions not only in ActivityNet-Captions dataset, e.g., 2966 in (0, 0.1] vs. 417 in (0.8, 0.9], but also in the real-life applications. For temporal grounding task, we are more likely to search for a short moment in a long video rather than search for a very long moment covering the entire video. Therefore we think that our improvement in short moments is useful and non-trivial in the setting of temporal grounding, and our auxiliary dual matching task by pair discrimination for a more discriminative feature is a good way to tackle this problem for short moments.